Highly Selective SAM–Nanowire Hybrid NO_2 Sensor: Insight into Charge Transfer Dynamics and Alignment of Frontier Molecular Orbitals

Martin W. G. Hoffmann, Joan Daniel Prades, Leonhard Mayrhofer, Francisco Hernandez-Ramirez, Tommi T. Järvi, Michael Moseler, Andreas Waag, and Hao Shen**

Organic–inorganic hybrid gas sensors can offer outstanding performance in terms of selectivity and sensitivity towards single gas species. The enormous variety of organic functionalities enables novel flexibility of active sensor surfaces compared to commonly used pure inorganic materials, but goes along with an increase of system complexity that usually hinders a predictable sensor design. In this work, an ultra-selective NO_2 sensor is realized based on self-assembled monolayer (SAM)-modified semiconductor nanowires (NWs). The crucial chemical and electronic parameters for an effective interaction between the sensor and different gas species are identified using density functional theory simulations. The theoretical findings are consistent with the experimentally observed extraordinary selectivity and sensitivity of the amine-terminated SnO_2 NW towards NO_2. The energetic position of the SAM–gas frontier orbitals with respect to the NW Fermi level is the key to ensure or impede an efficient charge transfer between the NW and the gas. As this condition strongly depends on the gas species and the sensor system, these insights into the charge transfer mechanisms can have a substantial impact on the development of highly selective hybrid gas sensors.

1. Introduction

The selective detection of a certain predefined gas species is the most critical requirement in different fields like pollution and food control, health care, security or industrial process control. However, predictive strategies towards the development of highly selective nanostructured gas sensors are still missing.[1] Organo-functionalized low dimensional materials could already show improved characteristics in this field[2–9] compared to commonly used purely inorganic materials or heterostructures that usually suffer from unspecific surface interactions with the target gases.[10–14] Here, we present a sensor system composed of semiconductor nanowire (NW) surfaces with defined organic self-assembled monolayers (SAMs) in order to accomplish exclusive chemical and electronic conditions for the selective detection of a single gas species. We demonstrate that SnO_2 NWs (see Figure S1) modified with amine terminated SAMs show both extraordinary selectivity and sensitivity towards NO_2 at room temperature. This system can not only serve as a novel efficient and selective NO_2 sensor, but also as a model system for the theoretical reconstruction of crucial sensor-target interactions. Our simulations reveal that an energy level alignment of the SAM-gas system with the Fermi level of the SAM–NW system is the key to understand and achieve high detection selectivity and are consistent with our experimentally observed results. The use of organic functionalities at semiconductor nanostructures in combination with a thorough simulation of the detailed chemical and electronic surface configuration thus shows a convincing potential for the development of theoretically designed selective gas sensors,[15] with flexible organic surface design and predictable response.

Gaseous nitrogen dioxide (NO_2) is one of the most dangerous and wide spread global pollutants, as it can produce ozone, acid rain and respiratory ailments.[16] Moreover it is believed to cause cancer due to its high reactivity with genetic material and organic solvents, forming nitrosamines.[17] NO_2 is produced by various ubiquitous combustion processes such as car engines, power plants and cigarette smoke and affects the human health already in tiny concentrations (ppb level).[18] Usually nitrogen oxide species in pollutant and toxic emissions are specified as NO_x due to the diversity of possible nitrogen oxidation states,

M. W. G. Hoffmann, Dr. J. D. Prades, Dr. F. Hernandez-Ramirez
Department of Electronics
University of Barcelona
E-08028, Barcelona, Spain
E-mail: dprades@el.ub.es

M. W. G. Hoffmann, Prof. A. Waag, Dr. H. Shen
Institut für Halbleitertechnik
Technische Universität Braunschweig
D-38106, Braunschweig, Germany
E-mail: h.shen@tu-bs.de

Dr. L. Mayrhofer, Dr. T. T. Järvi, Prof. M. Moseler
Fraunhofer Institute for Mechanics of Materials IWM
D-79108, Freiburg, Germany

M. W. G. Hoffmann, Dr. F. Hernandez-Ramirez
Department of Advanced Materials for Energy Applications
Catalonia Institute for Energy Research (IREC)
E-08930, Barcelona, Spain

DOI: 10.1002/adfm.201301478

and the inability of current cost-effective monitoring systems to discriminate among them. However, it is critical to distinguish NO and NO_2, which are the major fractions, as they exhibit different properties in terms of toxicity, biological impact and chemical reactivity.[17,19] All this makes this case a paradigmatic and unsolved problem in low-cost gas monitoring technology.

2. Results and Discussion

2.1. Experimental Approach for an Initial Sensor System

To develop a strategy for coherent experimental and theoretical gas sensor design, an optimal organic functionalization of SnO_2 NWs for selective NO_2 detection was first evaluated experimentally. The identified system then served as starting point to build up a theoretical NW–SAM–gas model and define critical parameters for selective sensing interactions. Amines, due to their electron donating character, were chosen as functional units to achieve strong surface–gas interactions with the electron affine NO_2 target (**Figure 1**a).[19] This process was supposed to affect the carrier concentration profile of the semiconductor NW and thus its resistance to give a measurable sensor response (Figure 1b).[20–24] Different kinds of SAMs with primary, secondary, tertiary and mixed amine terminals were immobilized on the SnO_2 NW surface (Figures 1a, S1, S2).[25] X-ray photoemission spectroscopy (XPS) of immobilized *N*-[3-(trimethoxysilyl)propyl]ethylenediamine **1** (en-APTAS) showed

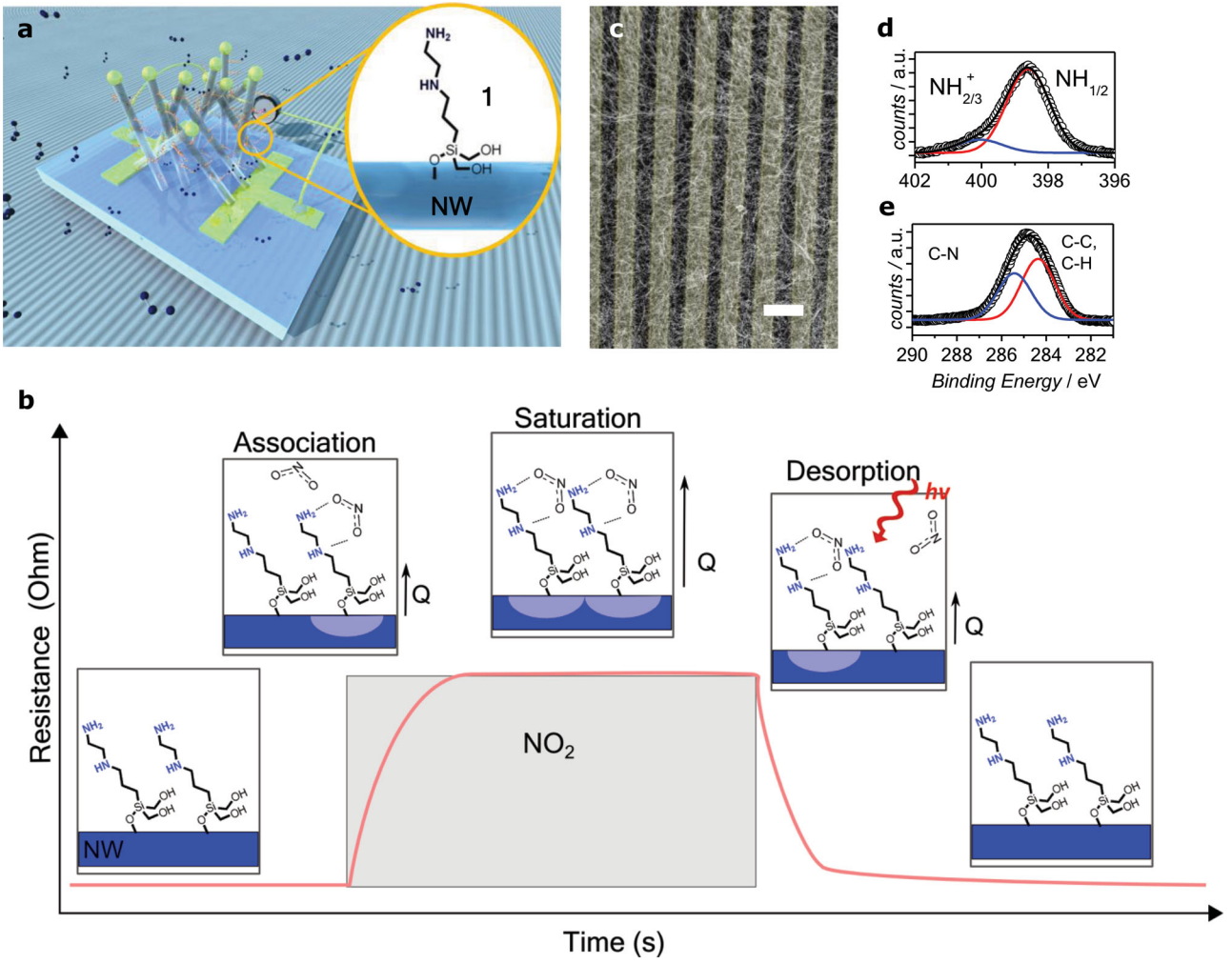

Figure 1. a) Schematic illustration of the selective NO_2 sensor. *N*-[3-(Trimethoxysilyl)propyl]ethylenediamine (en-APTAS 1) was immobilized on the surface of SnO_2 NWs which were directly grown on an interdigital gold electrode (5 µm spacings). The measured device resistance served as sensor signal. b) Schematic illustration of the NO_2 sensing mechanism by en-APTAS 1 modified NWs. With the introduction of NO_2, a SAM–gas interaction is established during the association process. The consequent electron transfer (Q) from the SAM to NO_2 is transduced to the NW and causes a charge depletion region that is monitored by an increasing sensor resistance. The depletion region is increased by additional NO_2-SAM interactions until saturation is reached. The cleaving of NO_2-SAM interactions by incident visible light during the desorption process leads to the initial unbound state and resistive character of the sensor. c) Scanning electron microscope (SEM) image of the en-APTAS 1 modified SnO_2 NWs with an average diameter of 47 ± 8 nm, grown on an interdigital electrode (scale bar, 10 µm). d) XPS N_{1s} of the en-APTAS 1 modified SnO_2 NWs showing binding energies of NH/NH_2 groups as well as small amounts of protonated NH_2^+/NH_3^+ groups that are shifted to higher binding energies in the N_{1s} spectra. e) Binding energies of C_{1s} spectra correspond to C–N and C–C/C–H groups of the SAM 1.

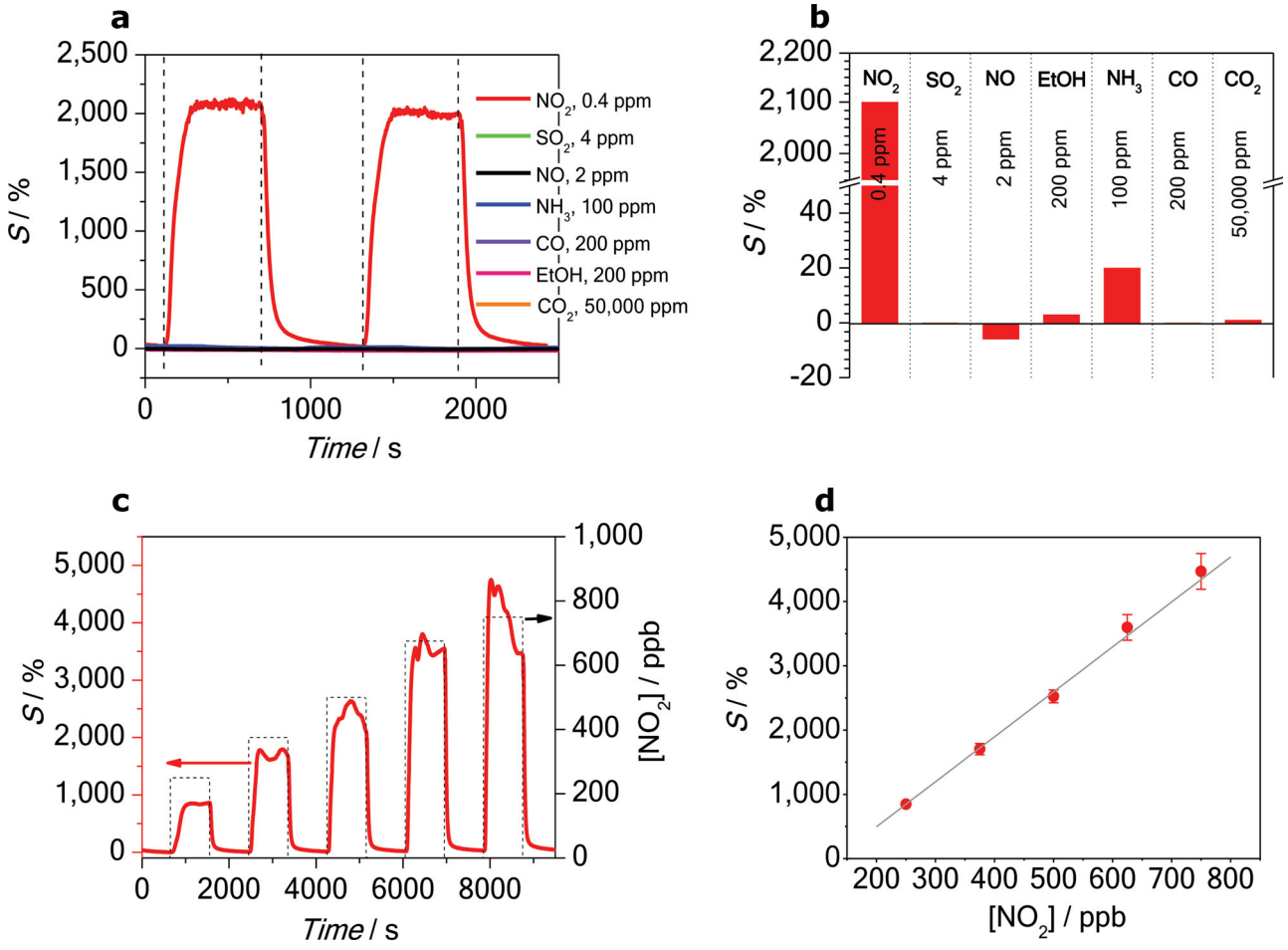

Figure 2. The en-APTAS **1** functionalized SnO_2 NW sensor measured under solar illumination (85 mW/cm^2). a) Pulses of 0.4 ppm NO_2, SO_2 (4 ppm), NO (2 ppm), NH_3 (100 ppm), ethanol (200 ppm), CO (200 ppm) and CO_2 (50,000 ppm). b) Summary of sensitivities towards the tested gases. c) Sensing response vs. different NO_2 concentrations ranging from 250 to 750 ppb in synthetic air. d) linear behaviour of the sensor response with different NO_2 concentrations.

the typical binding energies of the primary and secondary amine groups (NH/NH_2) in the N_{1s} and C_{1s} spectra, as well as a partial protonation (NH_2^+/NH_3^+) (Figures 1d,e). The successful immobilization of the amine SAM on the SnO_2 NW surface was further proved by Fourier-transform IR (FT-IR) analysis (Figure S1). In order to prove the selective detection of the NO_2 target, the gas sensing properties of all devices were tested towards small concentrations of NO_2 as well as high concentrations of other fossil combustion gases or interfering species (SO_2, NO, NH_3, EtOH, CO, and CO_2) (**Figure 2**a,b and Figure S2). The test gases were diluted in synthetic air and applied via a mass flow controller system into a sensor chamber with controllable gas flow. A constant current (100 nA) was applied to the sensor and the voltage was measured to monitor the resistive change of the semiconductor NWs. The sensitivity of the sensor is given as $S = [(R_{gas}/R_{air}-1)*100]$ [%]. To ensure a fast and complete recovery of the sensor signal, the active surface was illuminated through a quartz window by a solar simulator with constant illumination intensity (AM1.5; 85 mW/cm^2). All measurements were performed at room temperature.

All amine SAMs showed a very high sensitivity and selectivity towards a low NO_2 concentration (400 ppb; Figure 2, Figures S2a-c), whereas only small or mostly no response was observed for higher concentrations of the other gases (SO_2, NO, NH_3, ethanol, CO, and CO_2; concentrations between 2 ppm and 5%). Among all amines (see Supporting Information), the en-APTAS **1** functionalization with a primary and secondary group unified the best performance in both, sensitivity and selectivity, towards NO_2. With the introduction of 400 ppb NO_2, the resistance instantly increased to give a sensitivity of 2100%, whereas the other gases did not show any response (SO_2, CO, and CO_2) or very low values (NH_3, NO, ethanol) (Figures 2a,b). The low response towards 100 ppm of NH_3 (S = 20%) can be attributed to a protonation of the more basic amine functionalities (pK_a ~ 10.6) by the more acidic ammonia (pK_a = 9.2). Of particular interest was the low and negative sensitivity value towards 2 ppm NO gas (S = –6%). Cross sensitivity of NO_2 and NO is up to date a major issue in the analysis of NO_x mixtures produced in various combustion processes. The identification of a single nitrogen oxide species, here NO_2, is featured by our system in a very simple and cost effective configuration.

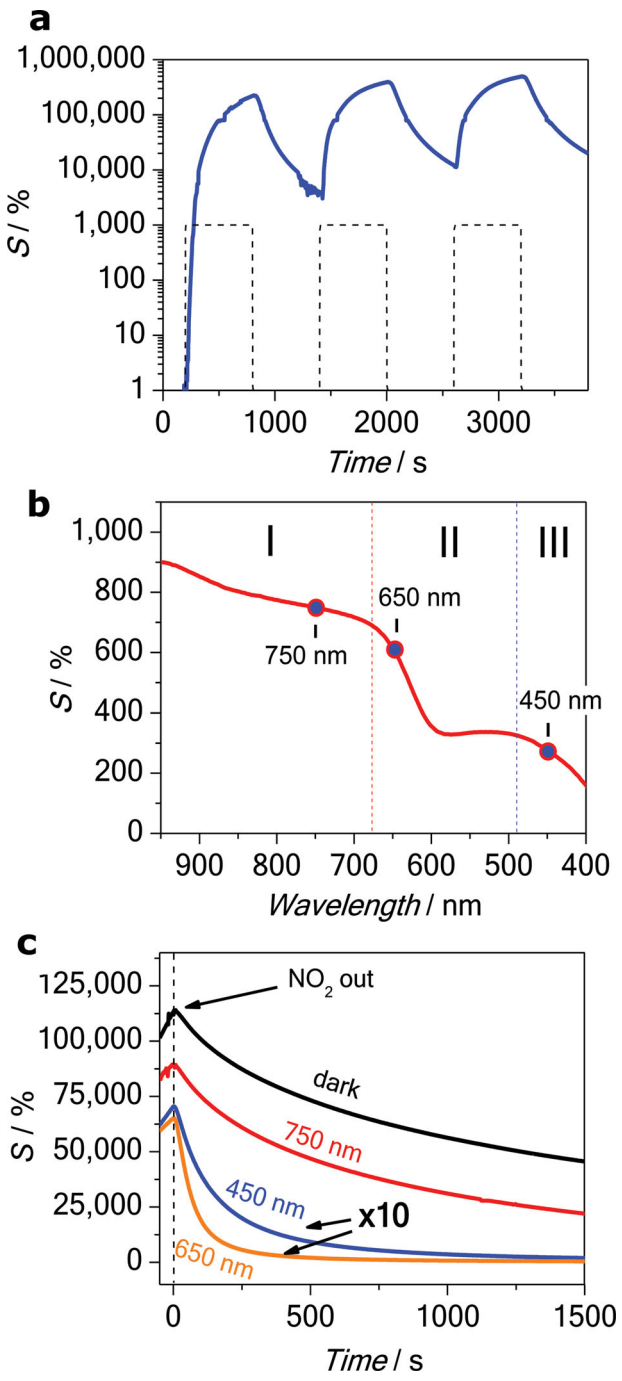

Figure 3. a) Pulses of 250 ppb NO_2 measured with an en-APTAS **1** functionalized SnO_2 NW sensor without illumination. b) Sensor recovery process after a pulse of NO_2 while sweeping of the incident light from 950 to 400 nm. After an almost constant resistance (I), two recovery processes can be identified starting at 680 (II) and 480 nm (III), respectively. c) Recovery processes after NO_2 pulses with illuminations of 450, 650, 750 nm and in dark conditions (position marked in Figure 3b), showing fast recovery for the two higher energy illuminations on one hand and slower and incomplete recovery for 750 nm and dark conditions on the other hand.

After switching the atmosphere from test gas back to pure synthetic air, the signal subsequently dropped down to the initial value before loaded with NO_2 gas. The quantitative sensing response was proportional to the appropriate NO_2 concentration (Figure 2c). Average response and recovery times were 110 and 75 s, respectively. A low NO_2 concentration of 250 ppb (minimum concentration of the experimental setup) could still be detected with a high sensitivity of 850% which implies that the system is capable of sensing NO_2 selectively within the range of critical values for human health (low ppb level).

The same gas sensing experiments performed in dark conditions revealed a slower but even stronger response towards NO_2 with a comparable selectivity and an extraordinary sensitivity of 225 000% for NO_2 concentrations as low as 250 ppb. In contrast to measurements under solar illumination, the response did not reach a signal saturation and the signal recovery was much slower (**Figure 3**a), causing a response accumulation when further NO_2 pulses were introduced. The incomplete sensor response does not allow a fast and quantitative analysis of the target gas in the dark. Thus, light illumination is obviously needed to achieve a fast and reversible sensor response as well as signal saturation. These findings indicate that the intermediate SAM–NO_2 species can be split by incident light, returning to the initial amine and resulting in a dynamic equilibrium of binding- and removal processes (signal saturation). Without illumination, SAM–NO_2 binding processes are ongoing without a coincidental NO_2 removal and thus the signal accumulates during NO_2 pulses without being saturated. In order to figure out the recovery characteristics of the bound SAM–NO_2 state, of the incident monochromatic light was swept from 950 to 400 nm after a NO_2 pulse. It was found that after an almost constant phase (Figure 3b, phase I), fast recovery processes started for wavelengths from 680 and 480 nm (Figure 3b, phase II and III). Both values are above the absorption edge of SnO_2 (<400 nm), proving that the gas detection mechanism does not directly involve SnO_2 as active sensing material, since recovery processes of wide band semiconductors need higher energy UV illumination to be activated.[26,27] Additionally, identical pulses of NO_2 where applied with different wavelengths of the three recovery phases (I, II, and III), as well as in dark conditions (Figure 3c). The measurements confirmed that an illumination between 450 and 650 nm is needed to remove the NO_2 species bound to the SAM molecules effectively to achieve a complete and fast sensor recovery. The weak binding interaction between the SAM and gas molecules allows for an easy signal recovery with lower energy input compared to conventional NW based gas sensors without amine functionalization. Due to the amine termination of the SAM, acid–base interactions with water could possibly have a detrimental influence on the sensor response and recovery characteristics, as well as on lifetime and stability.[25,28,29] However, experiments in humid air show that the sensor response to NO_2 is slightly reduced, but stable and fully reversible when the atmosphere is changed back to dry air (Figure S3).

2.2. Theoretical Identification of Crucial Sensor–Gas Interactions

Based on the initial experimental results, a theoretical model of the complete sensor system was developed within density functional theory (DFT) to simulate (i) the chemical bonding of the en-APTAS **1** SAM to the SnO_2 surface, the interaction of various gas molecules with the SAM ligand in the (ii) absence

and (iii) presence of the SnO_2 surface and finally (iv) the charge transfer process between adsorbed gas molecules and the SAM modified SnO_2 NW. In addition to the response of the sensor to NO_2, the absorption of NO and SO_2 was also theoretically examined in order to obtain further insight into the origin of the very high selectivity. It turns out that adsorption of NO_2 leads to charge transfer from the NW to the gas molecule. In this respect it is quite surprising that SO_2 shows no sensor response (Figure 2a,b), although it has similar oxidative and structural characteristics as NO_2. NO even induces a charge transfer opposite in sign to the NO_2 signal in agreement with the experimental findings. For both, experiment and theory, the (110) surface representing the lowest energy surface of SnO_2 was used.[30] Doping of SnO_2 with negative charge carriers was realized via incorporation of hydrogen atoms substituting oxygen atoms in the SnO_2 (Figure S9).[31]

DFT modeling revealed that bonding of the SAM to the SnO_2 surface via a single oxygen atom is the energetically favourable case and is used below (Figure S4). In the relaxed structure the SAM is tilted towards the SnO_2 surface. Different initial geometries for the free SAM–NO_2, SAM–SO_2 and SAM–NO system were used for structural relaxations in order to find the optimal SAM–gas geometries (Figures S5–7). The lowest energy geometries have SAM-gas binding energies E_b of –0.44 eV (NO_2), –0.83 eV (SO_2) and –0.48 eV (NO).

The optimal SAM–gas geometries were then combined with the optimized SAM-NW geometries. For the three-atomic gas molecules (NO_2, SO_2), bonding with the SAM at the optimal bonding site is sterically hindered by the influence of the NW surface as well as neighboring SAM ligands. As a consequence, NO_2 relaxes at the geometry with the second highest bonding strength near the secondary amine group with a binding energy of –0.26 eV and SO_2 relaxes at a position near the primary amine group at the head of the SAM corresponding to configuration 5 in Figure S6, with a binding energy of –0.71 eV. NO relaxes at the optimal bonding geometry also in presence of the NW surface (E_b = –0.24 eV). The charge transfer within the NW-SAM-gas system upon adsorption of the gas molecules was determined as

$$\Delta\rho(z) = \rho_{g-\mathrm{SAM}-\mathrm{SnO_2}}(z) - \rho_{\mathrm{SAM}-\mathrm{SnO_2}}(z) - \rho_g(z), \quad g = \mathrm{NO_2},\ \mathrm{SO_2},\ \mathrm{NO} \tag{1}$$

where $\rho_{g-\mathrm{SAM}-\mathrm{SnO_2}}$ is the electron density of the relaxed SAM-modified NW in the presence of the gas molecule g averaged over the SnO_2 (110) plane, $\rho_{\mathrm{SAM}-\mathrm{SnO_2}}$ and ρ_g are the averaged electron densities of the isolated SAM-NW system and the gas molecule with geometries from the relaxed NW-SAM-gas system. The coordinate along the (110)-direction is denoted by *z*. As can be seen from **Figure 4**a, the adsorption of NO_2 at the SAM bound to the SnO_2 surface leads to charge transfer from the NW via the SAM to the NO_2 molecule. A charge depletion zone extending into the NW backbone is observed. Charge transfer is also found after NO adsorption. However, here charge is transferred in the opposite direction, from the NO molecule via the SAM to the NW. On the other hand, the adsorption of SO_2 does not induce any noticeable charge variation in the NW. Merely a localized charge redistribution in the SAM–SO_2 part of the system is observed. Hence, our simulations suggest that while NO_2 adsorption leads to a decrease and NO adsorption to an increase of negative charge carriers in the NW, SO_2 has no impact, although it shows the strongest bonding to the SAM–NW system. Since SnO_2 is an n-type semiconductor, the simulations are consistent with the experimental observation of increasing and decreasing resistance in the presence of NO_2 and NO, respectively, while SO_2 does not lead to any considerable change (Figure 2a,b). Note that while the direction of charge transfer corresponds to the sensing measurement, the magnitude of the sensor signal being proportional to the device resistance cannot be obtained directly from DFT calculations.

Analyzing the density of states (DOS) of the SAM–NW system with adsorbed gas molecules, we found that NO_2 and NO adsorption lead to the formation of additional states directly at the NW–SAM Fermi level (Figure 4b). These states can be attributed to the LUMO in the case of NO_2, and in the case of NO to the HOMO of the corresponding gas–SAM system. Those states are mainly formed by the LUMO and HOMO of the isolated NO_2 and NO gas molecules as can be seen from Figure 4c, where we show the charge densities associated with the aforementioned wavefunctions of the NW–SAM–gas systems. As the DOS from Figure 4b shows, the NO_2–SAM LUMO becomes partially occupied and thus can take up charge carriers from the NW, contrary to the NO–SAM system for which the HOMO becomes partially depopulated by donating charge to the NW. Finally for SO_2, none of the frontier molecular orbitals is located at the Fermi level (Figure 4b) such that the occupations of the HOMO and LUMO of the gas–SAM system remain unaffected and no charge transfer is observed in this case.

To get a clear picture, we determined the HOMO and LUMO energy levels of the isolated SAM–gas systems in the absence of the NW and aligned their positions with the energy scale of the SAM-modified SnO_2. As reference for the alignment procedure the average electrostatic potentials at the cores of the carbon and nitrogen atoms at the backbone of the en-APTAS **1** molecule were used. As shown in Figure 4d, the LUMO of the NO_2–SAM system lies below the Fermi-level of the SAM-modified SnO_2. Hence charge transfer from the SnO_2 to the LUMO of the NO_2–SAM system is energetically favoured until LUMO and Fermi-level are aligned. In contrast, the NO-SAM system has a HOMO higher in energy than the Fermi-level of the SAM-modified SnO_2. Hence energy is gained by transferring charge from the HOMO of the NO–SAM system to the SnO_2. Finally, the LUMO of the SO_2–SAM system lies well above the Fermi-level and the HOMO lies well below the Fermi-level and so charge transfer is absent in agreement with the charge transfer simulations and sensing experiments. This analysis is extended to CO and CO_2 adsorbed on en-APTAS **1**. Determining the energies of the corresponding frontier orbitals (Figure 4d), the HOMOs are well below and the LUMOs are well above the SAM–NW Fermi level. Hence, as in the case of SO_2 charge transfer cannot occur for CO and CO_2, in agreement with our experimental results. In total, the simulations indicate that the key to explain the selectivity of the SAM modified sensor towards different gas molecules lies in the positions of the gas–SAM frontier molecular orbitals with respect to the Fermi level of SAM-modified SnO_2 NWs. This property guides

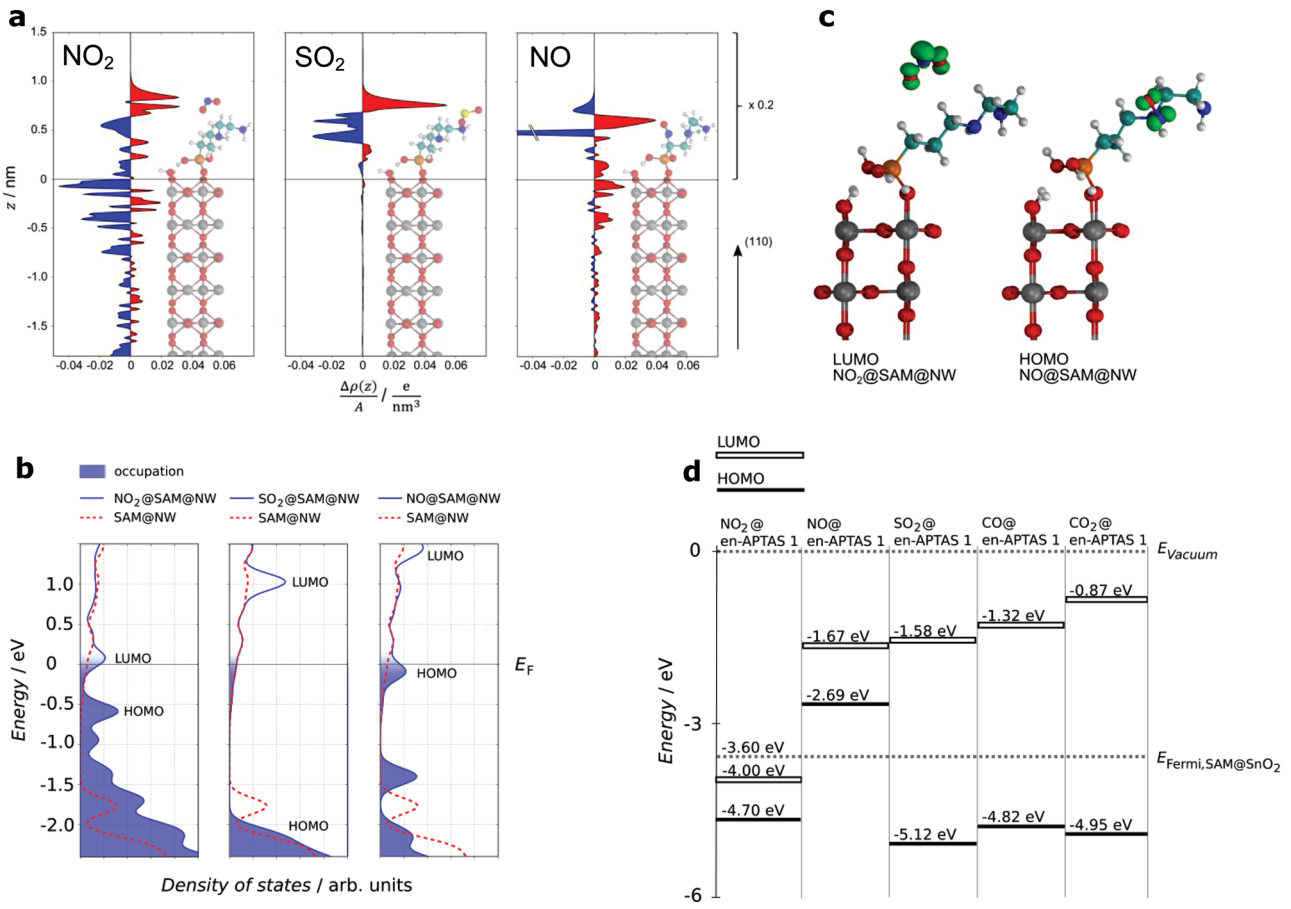

Figure 4. a) The change in averaged one-dimensional charge density $\Delta\rho(z)$ per surface area A along the (110) direction upon NO_2, SO_2 and NO adsorption on the en-APTAS **1** functionalized SnO_2 (110) surface for the energetically most favourable geometries. These geometries are shown as insets and are true to length scale. The electron charge is denoted by e. Regions of charge depletion are indicated by blue and regions of charge accumulation are indicated by red fillings. For clarity $\Delta\rho(z)$ has been scaled by a factor of 0.2 in the region outside the SnO_2. The SnO_2 surface (z = 0) is defined by the average position of the bridging oxygen atoms on the SnO_2 surface along the (110) direction. b) Density of states (DOS) of the en-APTAS **1** modified SnO_2 with adsorbed NO_2, SO_2 and NO. The Fermi levels of the different systems are set to 0 eV. For comparison the DOS of the en-APTAS **1** modified SnO2 NW without an adsorbed gas molecule (dashed red line) is shown in each graph. c) The charge densities of the wave functions corresponding to the peaks in the densities of states aligned with the Fermi levels from b are shown as green isosurfaces. The isosurfaces are drawn at a value of 0.075 e/Å^3. These are basically the LUMO of the NO_2 molecule, and the HOMO of the NO molecule. d) Energy diagram of the frontier orbitals of the two- and three-atomic gases adsorbed on en-APTAS **1**. Gases with HOMOs below and LUMOs above the Fermi level of the SAM-modified SnO_2 do not lead to a noticeable gas sensing signal in the experiments. NO_2 with the LUMO of the NO_2-en-APTAS **1** system below the Fermi level leads to an increasing sensor resistance whereas NO with the HOMO being above the Fermi level leads to a decreasing sensor resistance.

the way to the tailoring of SAM–nanowire surfaces towards highly selective gas sensing.

3. Conclusion

In conclusion, we demonstrated that the theoretical prediction of a SAM–NW hybrid sensor system is capable to provide an effective strategy for designing functionalized gas sensors through electronic structure calculations. The selectivity of the hybrid sensor is caused by a suitable alignment of the gas–SAM frontier molecular orbitals with respect to the SAM–NW Fermi-level. The present sensor is capable of detecting very low NO_2 concentrations in the ppb range qualitatively and quantitatively with relatively fast response and recovery time at room temperature. It fulfills the criteria for environmental pollution monitoring systems based on a very simple and cost effective device. Our work demonstrates that a systematic organic surface design of semiconductor nanostructures shows great potential in solving the selectivity issue, which is the main obstacle of current gas sensor technologies. On the long term, this knowledge could lead to a strategy with which a tailored and flexible design of highly precise artificial noses is enabled.

4. Experimental Section

Preparation of SnO_2/en-APTAS 1 Sensors: The as-prepared SnO_2 NWs (average diameter 40–60 nm) grown on Al_2O_3 substrates with pre patterned interdigital gold electrodes (5 µm spacings) were cleaned in oxygen plasma for 1 min to remove surface contaminations and provide oxygen groups on the surface for the condensation reaction. Subsequently, the sample was immersed in a 1% ethanol solution of

en-APTAS **1** (ABCR GmbH), which was stirred for 6 h. After removal, the sample was subsequently rinsed with ethanol and dried in a vacuum oven for 1 h at 60 °C.

Gas Sensing Experiments: The SnO_2/en-APTAS **1** samples where electrically contacted via wire bonding and placed in a gas chamber with gas in-, outlet and a quartz window for external illumination. The gas flow was controlled by a flow control system (Gometrics MGP-2) and the sensor signal was monitored by a SMU (Keithley 2400) that was controlled by self-programmed LabVIEW software (National Instruments Inc.). The sensor was illuminated with simulated sunlight (AM1.5, 85 mW/cm^2) through a quartz window. All gas sensing experiments were performed at room temperature.

DFT Simulations: The modified SnO_2 was modeled as slab terminated by (110) surfaces and consisting of 11 layers amounting to a thickness of 38.378 Å for the relaxed slab. Since the sensor is exposed to humidity during preparation and operation dissociative adsorption of H_2O on the SnO_2 surface has been assumed.[32] From the relaxed SnO_2 bulk structure the dimensions of the surface unit cell of 6.714 Å $\times$ 6.346 Å were extracted. The considered unit cell is depicted in Figure S4a. For the charge transfer calculations one oxygen atom per unit cell in the center of the SnO_2 slab was substituted by hydrogen in order to model n-type doping,[31] see Figure S9a. Periodic boundary conditions were employed in all directions. Vacuum layers of at least 25 Å were used to separate the slabs. We used completely symmetric setups with respect to the upper and lower slab surfaces in order to suppress artifacts due to electrostatic interactions between neighboring slabs. The en-APTAS **1** SAM was modeled by one ligand at each SnO_2 surface in the unit cell. For the simulations involving en-APTAS **1** molecules in the absence of SnO_2, all unsaturated bonds of the molecule have been terminated by OH groups.

All calculations were performed within the PBE+U framework using U = 3.5 eV[31] with the Vienna ab-initio Simulation Package (VASP).[33] Here, we used the PAW method and pseudopotentials,[34,35] an energy cutoff of 400 eV, a Monkhorst-Pack k-point sampling of 3 in the lateral directions, and Gaussian smearing with a width of 0.1 eV. For relaxations a force cutoff of 0.015 eV/Å was used. Dispersion forces were taken into account by using the semi-empirical DFT-D2 method of Grimme[36] as implemented in VASP. Sn atoms have been excluded from the dispersion correction in order to preserve the very good agreement between the PBE+U and the experimental values[37] of the SnO_2 lattice constants.

For the density of states (DOS) calculations the same DFT parameters as above were used except of using a Monkhorst-Pack k-point sampling of 9 in the lateral directions. The DOS was obtained by convolution of the DFT-eigenvalues with a Gaussian of width 0.10 eV.

Supporting Information

Supporting Information is available from the Wiley Online Library or from the author.

Acknowledgments

M. W. G. H. acknowledges the German Academic Exchange Service (DAAD) for the PhD grant (D/11/43761). H. S. is thankful to the BMBF-NanoFutur project (FKZ 03×5512). The authors are thankful to Dr. Sven Barth for the synthesis of SnO_2 nanowires, Dr. Lorenzo Calvo Barrio for XPS measurements and Dr. Nuria Ferrer for support in FT-IR measurements. L. M. and T. T. J. thank Marcus Rosenblatt for support in generating the initial molecule–SAM geometries. The calculations have been performed on the Joe1 cluster at Fraunhofer IWM and Juropa at the Jülich Supercomputing Centre (JSC).

Received: April 30, 2013
Revised: June 4, 2013
Published online: August 16, 2013

[1] R. M. Penner, *Annu. Rev. Anal. Chem.* **2012**, *5*, 461–85.
[2] S. Barth, F. Hernandez-Ramirez, J. D. Holmes, A. Romano-Rodriguez, *Prog. Mater. Sci.* **2010**, *55*, 563–627.
[3] S. Rumyantsev, G. Liu, M. S. Shur, R. Potyrailo, A. Balandin, *Nano Lett.* **2012**, *12*, 2294–2298.
[4] A. Gulino, T. Gupta, P. G. Mineo, M. E. van der Boom, *Chem. Commun.* **2007**, *2*, 4878–4880.
[5] A. Palaniappan, S. Moochhala, F. E. H. Tay, N. C. L. Phua, X. Su, *Sens. Actuat. B* **2008**, *133*, 241–243.
[6] Y. Engel, R. Elnathan, A. Pevzner, G. Davidi, E. Flaxer, F. Patolsky, *Angew. Chem. Int. Ed.* **2010**, *49*, 6830–6835.
[7] M. C. McAlpine, H. D. Agnew, R. D. Rohde, M. Blanco, H. Ahmad, A. D. Stuparu, W. A. Goddard, J. R. Heath, *J. Am. Chem. Soc.* **2008**, *130*, 9583–9589.
[8] W. Yuan, A. Liu, L. Huang, C. Li, G. Shi, *Adv. Mater.* **2013**, *25*, 766–771.
[9] L. Torsi, G. M. Farinola, F. Marinelli, M. C. Tanese, O. H. Omar, L. Valli, F. Babudri, F. Palmisano, P. G. Zambonin, F. Naso, *Nature Mater.* **2008**, *7*, 412–417.
[10] M. W. G. Hoffmann, A. Eldin Gad, J. Daniel Prades, F. Hernandez-Ramirez, R. Fiz, H. Shen, S. Mathur, *Nano Energy* **2013**, 1–9.
[11] G. F. Fine, L. M. Cavanagh, A. Afonja, R. Binions, *Sensors* **2010**, *10*, 5469–5502.
[12] F. Hernandez-Ramirez, J. D. Prades, A. Tarancon, S. Barth, O. Casals, R. Jimenez-Diaz, E. Pellicer, J. Rodriguez, J. R. Morante, M. A. Juli, S. Mathur, A. Romano-Rodriguez, *Adv. Funct. Mater.* **2008**, *18*, 2990–2994.
[13] G. Korotcenkov, *Mater. Sci. Eng. B* **2007**, *139*, 1–23.
[14] J. D. Prades, R. Jimenez-Diaz, F. Hernandez-Ramirez, S. Barth, A. Cirera, A. Romano-Rodriguez, S. Mathur, J. R. Morante, *Appl. Phys. Lett.* **2008**, *93*, 123110.
[15] B. Kumar, K. Min, M. Bashirzadeh, A. Barati Farimani, M.-H. Bae, D. Estrada, Y. D. Kim, P. Yasaei, Y. D. Park, E. Pop, N. R. Aluru, A. Salehi-Khijin, *Nano Lett.* **2013**, DOI 10.1021/nl304734g.
[16] D. Zhang, Z. Liu, C. Li, T. Tang, X. Liu, S. Han, B. Lei, C. Zhou, *Nano Lett.* **2004**, *4*, 1919–1924.
[17] R. V. Cooney, P. D. Ross, G. L. Bartolini, J. Ramseyer, *Environ. Sci. Technol.* **1987**, *21*, 77–83.
[18] Directive 2008/50/EC of the European Parliament and of the Council, **2008**.
[19] M. D. Bartberger, W. Liu, E. Ford, K. M. Miranda, C. Switzer, J. M. Fukuto, P. J. Farmer, D. a Wink, K. N. Houk, *Proc. Natl. Acad. Sci.* **2002**, *99*, 10958–10963.
[20] D. Qi, W. Chen, X. Gao, L. Wang, S. Chen, K. P. Loh, A. T. S. Wee, *J. Am. Chem. Soc.* **2007**, *129*, 8084–8085.
[21] K. Yokota, K. Takai, T. Enoki, *Nano Lett.* **2011**, *11*, 3669–3675.
[22] M. F. Calhoun, J. Sanchez, D. Olaya, M. E. Gershenson, V. Podzorov, *Nature Mater.* **2008**, *7*, 84–89.
[23] S. Lacher, Y. Matsuo, E. Nakamura, *J. Am. Chem. Soc.* **2011**, *133*, 16997–17004.
[24] D. Boudinet, M. Benwadih, S. Altazin, J.-M. Verilhac, E. De Vito, C. Serbutoviez, G. Horowitz, A. Facchetti, *J. Am. Chem. Soc.* **2011**, *133*, 9968–9971.
[25] Y. Cui, Q. Wei, H. Park, C. M. Lieber, *Science* **2001**, *293*, 1289–1292.
[26] J. D. Prades, F. Hernandez-Ramirez, R. Jimenez-Diaz, M. Manzanares, T. Andreu, A. Cirera, A. Romano-Rodriguez, J. R. Morante, *Nanotechnology* **2008**, *19*, 465501.
[27] B. P. J. de Lacy Costello, R. J. Ewen, N. M. Ratcliffe, M. Richards, *Sens. Actuat. B* **2008**, *134*, 945–952.
[28] K. Bradley, J. Cumings, A. Star, J.-C. P. Gabriel, G. Grüner, *Nano Lett.* **2003**, *3*, 639–641.
[29] O. Kuzmych, B. L. Allen, A. Star, *Nanotechnology* **2007**, *18*, 375502.

[30] M. Batzill, U. Diebold, *Prog. Surf. Sci.* **2005**, *79*, 47–154.
[31] A. K. Singh, A. Janotti, M. Scheffler, C. G. Van de Walle, *Phys. Rev. Lett.* **2008**, *101*, 1–4.
[32] K. R. Hahn, A. Tricoli, G. Santarossa, A. Vargas, A. Baiker, *Langmuir* **2012**, *28*, 1646–1656.
[33] G. Kresse, J. Furthmüller, *Phys. Rev. B* **1996**, *54*, 11169–11186.
[34] G. Kresse, *Phys. Rev. B* **1999**, *59*, 1758–1775.
[35] P. Blöchl, *Phys. Rev. B* **1994**, *50*, 17953–17979.
[36] S. Grimme, *J. Comp. Chem.* **2006**, *17*, 1787–1799.
[37] W. H. Baur, A. A. Khan, *Acta Cryst. B* **1971**, *27*, 2133–2139.